

# A 0.0045-mm<sup>2</sup> 32.4- $\mu$ W Two-Stage Amplifier for pF-to-nF Load Using CM Frequency Compensation

Zushu Yan, *Student Member, IEEE*, Wei Wang, Pui-In Mak, *Senior Member, IEEE*,  
Man-Kay Law, *Member, IEEE*, and Rui P. Martins, *Fellow, IEEE*

**Abstract**—This brief reports an embedded capacitor multiplier (CM) frequency compensation technique to realize an extremely compact micropower two-stage amplifier for wide capacitive load ( $C_L$ ) drivability. It features: 1) a valuable left half-plane zero to enhance the closed-loop stability over a wide range of  $C_L$ ; 2) no extra bias circuit and power, as the CM is embedded into the first stage of the amplifier, and 3) only one very small (subpicofarad) compensation capacitor improving the transient settling and area efficiency. Detailed analytical treatments of the amplifier offer the critical insights for device sizing and optimization. Fabricated in 0.18- $\mu$ m CMOS, the amplifier measures 3.06-MHz unity-gain frequency (UGF), 1.76-V/ $\mu$ s average slew rate (SR), and 74° phase margin (PM) at 20-pF  $C_L$ , and 0.22-MHz UGF, 0.049-V/ $\mu$ s SR, and 59.8° PM at 15-nF  $C_L$ . The die size is 0.0045 mm<sup>2</sup>, and power is 32.4  $\mu$ W at 1.2 V. Competitive large- and small-signal figures of merit are achieved with respect to the state of the art.

**Index Terms**—Capacitive load, capacitor multiplier (CM), CMOS, frequency compensation, stability, two-stage amplifier.

## I. INTRODUCTION

**E**XTRREMELY compact micropower CMOS amplifiers with wide capacitive load ( $C_L$ ) drivability have found extensive applications in chemical sensors and liquid crystal display drivers [1], [2]. For amplifiers having three or more stages, their performances are tightly related to the frequency compensation scheme applied [3]. In fact, very few three-stage amplifiers are capable to drive pF-to-nF  $C_L$  at small power and area, due to the closed-loop stability constraints at either light or heavy  $C_L$  [4]. In contrast, two-stage amplifiers exhibit simpler tradeoffs among the major metrics such as dc gain, gain-bandwidth (GBW) product, power and area with frequency compensation. However, most existing frequency compensation schemes for the simple two-stage Miller amplifier were focused on eliminating the unwanted right half-plane zero, rather than extending the range of  $C_L$  drivability [5].

Manuscript received May 22, 2014; revised August 26, 2014; accepted November 1, 2014. Date of publication November 10, 2014; date of current version March 1, 2015. This work was supported in part by the University of Macau and Macau Science and Technology Development Fund (FDCT) under Grant 015/2012/A1 and the State Key Laboratory Fund. This brief was recommended by Associate Editor T. Ge.

Z. Yan, W. Wang, P.-I. Mak, and M.-K. Law are with the State Key Laboratory of Analog and Mixed-Signal VLSI and the Faculty of Science and Technology, Department of Electrical and Computer Engineering (ECE), University of Macau, Macau, China (e-mail: pimak@umac.mo).

R. P. Martins is with the State Key Laboratory of Analog and Mixed-Signal VLSI and the Faculty of Science and Technology, Department of Electrical and Computer Engineering (ECE), University of Macau, Macau, China, and also with the Instituto Superior Técnico, Universidade de Lisboa, 1049-001 Lisboa, Portugal (e-mail: rmartins@umac.mo).

Color versions of one or more of the figures in this brief are available online at <http://ieeexplore.ieee.org>.

Digital Object Identifier 10.1109/TCSII.2014.2368972

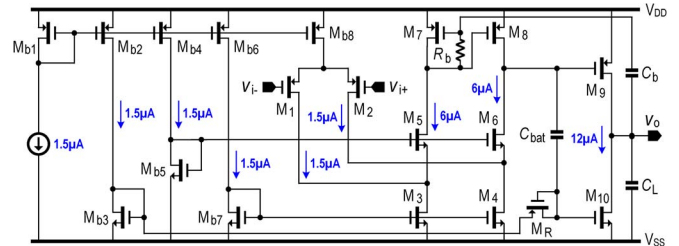


Fig. 1. Schematic of the proposed two-stage amplifier with embedded CM frequency compensation.

In this brief, we report a two-stage amplifier capable of driving a wide range of  $C_L$ , while achieving high power and area efficiencies. Previously, current buffer Miller compensation (CBMC) was optimized to realize a two-stage amplifier stable for any  $C_L$  [6]. However, to attain the small  $C_L$  stability, the current buffer has to dissipate a significant amount of power to push up the associated parasitic pole, and the measured step response at 10-pF  $C_L$  still exhibited a superimposed high-frequency ringing. Moreover, when  $C_L$  becomes heavy enough ( $> 100$  pF), the Miller capacitor must be increased to uphold the first-stage dc gain [6]. A large Miller capacitor penalizes not only the die area but also the power and slew rate (SR). To alleviate such tradeoffs, a capacitor multiplier (CM) can be applied to reduce the physical size of the capacitor and power. The current-mirror-based CM in [7] features simple realization, but it was hard to achieve a high multiplication factor under low power budget. Although there were many other alternatives [8] that can boost the multiplication factor by at least one order of magnitude, they inevitably produced low-frequency poles that limit the amplifier's GBW. In addition, existing current-buffers or CM realizations require add-on bias circuits, while inducing extra voltage offset, noise, and parasitic capacitances [8].

The described two-stage amplifier is based on the embedded CM frequency compensation scheme [8], but is architecturally improved via exploring a new design freedom to eliminate the GBW-limiting shunt compensation capacitor, while preserving the stability at small  $C_L$ . A modified class-AB output stage is also proposed to reduce the parasitic capacitance and save power. A complete *local feedback loop* (LFL) analysis [4] and a design procedure are proposed to optimize the performance of the amplifier over a wide range of  $C_L$ .

## II. PROPOSED TWO-STAGE AMPLIFIER WITH EMBEDDED CM FREQUENCY COMPENSATION

### A. Schematic

The schematic of the proposed two-stage amplifier with embedded CM frequency compensation is depicted in Fig. 1.

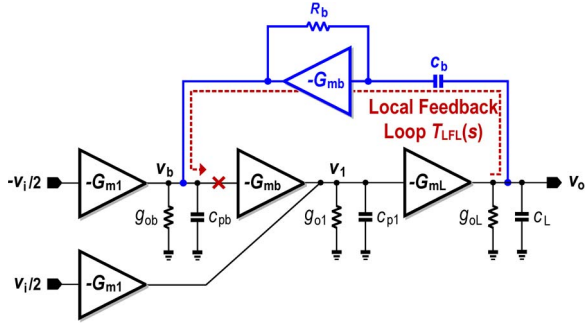


Fig. 2. Small-signal equivalent model of the proposed two-stage amplifier.

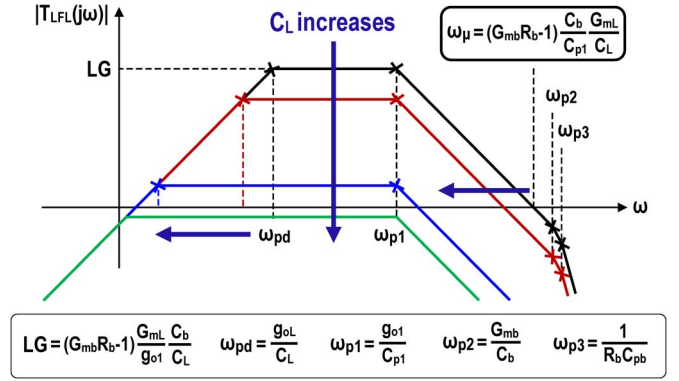
The first stage uses a folded-cascode structure ( $M_1 - M_8$  and  $M_{b8}$ ). The embedded CM is realized via  $R_b$ ,  $C_b$  and the reuse of the current mirror  $M_{7-8}$ . Unlike the realization in [8] entailing an extra compensation capacitor,  $C_b$  is solely responsible here for saving area and avoiding GBW reduction, particularly at large  $C_L$ . In addition, the light  $C_L$  drivability is not sacrificed because of the design freedom given by the embeddable CM, which will be detailed later.  $M_9$  and  $M_{10}$  form the output stage of the amplifier. In order to obtain symmetrical rising and falling SRs, a class-AB output stage is employed, and it is realized by adding  $C_{bat}$  and a diode-connected PMOS transistor  $M_R$  [9]. During the dynamic operation, the first stage's output will vary noticeably. Since  $M_R$  operates as an extremely large resistor, the time entailed to (dis)charge  $C_{bat}$  will be quite long. Hence, the voltage variation at the gate of  $M_9$  can be transferred to that of  $M_{10}$  with negligible loss.  $M_{b1} - M_{b8}$  form the basic current sources and mirrors, providing a proper bias current for the amplifier.

Fig. 2 depicts the amplifier's small-signal equivalent model. The two  $G_{m1}$  represent the transconductances of  $M_1$  and  $M_2$ .  $G_{mb}$  is the transconductance of  $M_{7-8}$ , while  $G_{mL}$  is the sum of  $M_9$  and  $M_{10}$  transconductances, accounting the ac effect of the class-AB output stage. The output conductance of each stage is denoted by  $g_{ob}$ ,  $g_{o1}$ , and  $g_{oL}$ , respectively.  $C_{pb}$ ,  $C_{p1}$ , and  $C_{p2}$  lumped into the load capacitor  $C_L$  model the parasitic capacitance at the corresponding nodes. The small  $C_b$  amplified by the embedded CM generates the required effective capacitance, which via the LFL ensures the two poles associated with  $v_1$  and  $v_o$  to split apart, producing widely spaced dominant and nondominant poles under light-to-medium  $C_L$  conditions.

### B. LFL Transfer Function

Conventional direct circuit analysis [4] cannot offer enough insights to optimize the amplifier's pole-zero arrangement when analyzing the stability of the amplifier over a wide range of  $C_L$ . The LFL analysis is employed here to guide the design phase, particularly at light- $C_L$  condition. As shown in Fig. 2, the LFL induced by the embedded CM is broken at node  $v_b$ . In addition to the assumption, i.e.,  $1/G_{mb} < R_b \ll 1/g_{ob}$ , for the embeddable CM, the LFL transfer function  $T_{LFL}(s)$  is derived, assuming that the gain of each stage is  $\gg 1$ , and  $C_{pb}$ ,  $C_{p1} \ll C_b \ll C_L$ , i.e.,

$$T_{LFL}(s) \approx \frac{-sG_{mL}(G_{mb}R_b - 1)C_b}{g_{o1}g_{oL} \left(1 + \frac{s}{\omega_{pd}}\right) \left(1 + \frac{s}{\omega_{p1}}\right) \left(1 + \frac{s}{\omega_{p2}} + \frac{s^2}{\omega_{p2}\omega_{p3}}\right)}. \quad (1)$$


 Fig. 3. LFL magnitude responses of the proposed two-stage amplifier under increasingly large  $C_L$ .

The conceptual magnitude responses of  $T_{LFL}(s)$  are shown in Fig. 3 over different values of  $C_L$ . The LFL's dominant pole is  $\omega_{pd}$ , while the first nondominant pole is  $\omega_{p1}$ .  $\omega_{\mu}$  is the LFL's UGF, and the other two high-frequency poles stemming from the embedded CM are  $\omega_{p2}$  and  $\omega_{p3}$ , respectively, which can be configured in a complex form to boost the LFL's phase margin (PM).

As illustrated in Fig. 3,  $\omega_{\mu}$  might locate close to  $\omega_{p2}$  and  $\omega_{p3}$  under a small  $C_L$ . If  $C_L$  is further decreased, the LFL's PM will deteriorate and degrade the LFL's stability, which imposes a significant magnitude peak in the overall transfer function of the amplifier. In the time domain, this will result in the step response exhibiting a long-lasting high-frequency oscillation [4]. To quantify the limit of low  $C_L$  drivability, the PM of the LFL, i.e.,  $PM_{LFL}$ , is calculated as

$$PM_{LFL} \approx 90^\circ - \tan^{-1} \frac{\frac{\omega_{\mu}}{\omega_{p2}}}{1 - \frac{\omega_{\mu}^2}{\omega_{p2}\omega_{p3}}}. \quad (2)$$

Solving (2) and substituting the expressions of  $\omega_{\mu}$ ,  $\omega_{p2}$ , and  $\omega_{p3}$ , the minimum  $C_L$  under a given  $PM_{LFL}$  is given by

$$C_{L\_min} \approx \frac{2(G_{mb}R_b - 1)G_{mL}R_b C_b}{\left(\sqrt{1 + \frac{4G_{mb}R_b}{(\tan PM_{LFL})^2} \frac{C_{pb}}{C_b}} - 1\right) \tan PM_{LFL}} \frac{C_{pb}}{C_{p1}} \quad (3)$$

where  $C_{L\_min}$  is not much vulnerable to process variations because  $C_{pb}$  is mainly determined by the gate capacitance of  $M_8$  that partially tracks  $C_{p1}$  (mostly arises from  $M_9$  and  $M_{10}$ ). To enhance the small  $C_L$  drivability, it was proposed in [8] to upscale  $C_{p1}$  via shunting an extra capacitor. Although the MOS capacitor (MOSCAP) realization incurs less area overhead, it substantially lowers the position of  $\omega_{p1}$ , thereby limiting the GBW. Particularly, as  $C_L$  becomes very large,  $\omega_{p1}$  comes into the first nondominant pole of the amplifier. Instead, the approach of selecting a smaller  $G_{mb}R_b - 1$  is explored in the proposed amplifier to balance the light  $C_L$  drivability with a large GBW.

Since  $\omega_{\mu}$ ,  $\omega_{p2}$ , and  $\omega_{p3}$  control the high-frequency portion of the amplifier's overall transfer function while  $\omega_{\mu}$  determines its first nondominant pole [4], a larger  $\omega_{\mu}$  results in a larger PM for the amplifier. When  $C_L$  is increased,  $\omega_{\mu}$  moves toward lower frequencies, as shown in Fig. 3. Although  $PM_{LFL}$  is improved, the amplifier's PM is degraded. The trend continues until the

midband LFL gain (LG) becomes no more than unity, which is expressed as

$$LG = (G_{mb}R_b - 1) \frac{G_{mL}C_b}{g_{o1}C_L} \leq 1. \quad (4)$$

As LG continues to reduce with increasingly large  $C_L$ , the LFL completely fails to shape the amplifier's frequency response, i.e., the amplifier degenerates into a simple two-stage amplifier without Miller compensation. The overall transfer function should then be resorted to assess the stability.

### C. Overall Transfer Function

As the wide-range  $C_L$  variation forces the LFL to be either effective or ineffective under different scenarios, the overall transfer function of the proposed amplifier should be studied according to different cases.

1) *Case 1:* When  $C_L$  is small ( $LG \gg 1$ ), the LFL takes control over the frequency response below  $\omega_\mu$ . The overall transfer function  $A_v(s)$  can be calculated as

$$A_v(s) \approx \frac{A_{DC} \left(1 + \frac{s}{\omega_z}\right)}{\left(1 + \frac{s}{\omega_d}\right) \left(1 + \frac{s}{\omega_\mu} + \frac{s^2}{\omega_\mu\omega_{p2}} + \frac{s^3}{\omega_\mu\omega_{p2}\omega_{p3}}\right)} \quad (5)$$

where  $A_{DC}$  is the dc gain  $G_{m1}G_{mL}/g_{o1}g_{oL}$ ;  $\omega_d$  is the dominant pole  $g_{o1}g_{oL}/G_{mL}(G_{mb}R_b - 1)C_b$ ; and the GBW is  $G_{m1}/((G_{mb}R_b - 1)C_b)$ . A useful left half-plane (LHP) zero  $\omega_z = 2G_{mb}/[(G_{mb}R_b + 1)C_b]$  is created, which can be used to improve the PM of the amplifier, i.e.,  $PM_{overall}$ , at light-to-medium  $C_L$  conditions. Unlike CBMC that relies on the LFL to create an LHP zero, the presence of such LHP zero is due to the existence of the direct feedforward signal path from the input to the output formed by  $R_b$  and  $C_b$  (see Fig. 2). As previously discussed, for small values of  $C_L$  that can maintain a reasonable  $PM_{LFL}$ , the amplifier shows enough  $PM_{overall}$  as  $\omega_\mu$ ,  $\omega_{p2}$ , and  $\omega_{p3}$  locates much higher than the GBW.

If  $C_L$  is large to reduce  $\omega_\mu$  to be much less than  $\omega_{p2}$  and  $\omega_{p3}$  while still ensures  $LG \gg 1$ , it means that the first nondominant pole of the amplifier, i.e.,  $\omega_\mu$ , can be factored out from the third-order polynomial in (5), simplifying  $A_v(s)$  to

$$A_v(s) \approx \frac{A_{DC} \left(1 + \frac{s}{\omega_z}\right)}{\left(1 + \frac{s}{\omega_d}\right) \left(1 + \frac{s}{\omega_\mu}\right) \left(1 + \frac{s}{\omega_{p2}} + \frac{s^2}{\omega_{p2}\omega_{p3}}\right)} \quad (6)$$

and  $PM_{overall}$  is given by

$$PM_{overall} \approx 90^\circ - \tan^{-1} \frac{GBW}{\omega_\mu} + \tan^{-1} \frac{GBW}{\omega_z} - \tan^{-1} \frac{\frac{GBW}{\omega_{p2}}}{1 - \frac{GBW^2}{\omega_{p2}\omega_{p3}}}. \quad (7)$$

As  $C_L$  is increased,  $\omega_\mu$  is reduced, while  $\omega_d$ ,  $\omega_z$ ,  $\omega_{p2}$ , and  $\omega_{p3}$  all remain unchanged, resulting in a lower  $PM_{overall}$ .

2) *Case 2:* When  $C_L$  is exceedingly large and forces  $LG \ll 1$ , the amplifier can be well approximated by a two-pole system, and the overall transfer function is given by

$$A_v(s) \approx \frac{A_{DC}}{\left(1 + \frac{s}{\omega_{pd}}\right) \left(1 + \frac{s}{\omega_{p1}}\right)} \quad (8)$$

where  $\omega_{pd}$  and  $\omega_{p1}$  correspond to the dominant and nondominant poles of the amplifier, respectively, and the GBW is  $G_{m1}G_{mL}/g_{o1}C_L$ .  $PM_{overall}$  is reformulated into

$$PM_{overall} \approx 90^\circ - \tan^{-1} \frac{GBW}{\omega_{p1}} = 90^\circ - \tan^{-1} \frac{G_{m1}G_{mL}G_{P1}}{g_{o1}^2 C_L}. \quad (9)$$

If  $C_L$  is further increased,  $\omega_{pd}$  will continue to reduce in frequency and the GBW follows. As  $\omega_{p1}$  is fixed,  $PM_{overall}$  is improved, and the amplifier becomes more stable. Hence, the proposed amplifier is unconditionally stable for any larger  $C_L$ .

3) *Case 3:* The aforementioned analysis of  $PM_{overall}$  versus  $C_L$  implies that there is a minimum  $PM_{overall}$ , i.e.,  $PM_{overall\_min}$  that occurs at  $LG = 1$ . The corresponding  $C_L$  is given by

$$C_L = \frac{G_{mL}(G_{mb}R_b - 1)C_b}{g_{o1}}. \quad (10)$$

Intuitively, this condition can be explained as the LFL just begins to lose the control over the amplifier's frequency response, and it contributes equally with the output stage to form the dominant pole of the amplifier. Thus,  $\omega_{pd}$  shifts to  $g_{oL}/2C_L$ , while  $\omega_{p1}$  is moved up to  $2g_{o1}/C_{p1}$ . Substituting (10) into (9) with the shifted  $\omega_{pd}$  and  $\omega_{p1}$ ,  $PM_{overall\_min}$  is evaluated as

$$PM_{overall\_min} = \tan^{-1} \frac{4g_{o1}(G_{mb}R_b - 1)C_b}{G_{m1}C_{p1}}. \quad (11)$$

There are several ways to achieve a good  $PM_{overall\_min}$ . One possibility is to limit the gain of the first stage, while degrading the offset and noise performances of the amplifier. In addition,  $C_{p1}$  can be reduced to improve  $PM_{overall\_min}$  at the expense of the small  $C_L$  drivability. However, the optimum solution would be to preserve a reasonably large  $(G_{mb}R_b - 1)C_b$ , which is the major advantage of the proposed embedded CM compensation allowing the use of a small  $C_b$  and therefore less  $G_{mb}$  (i.e., less power), when compared with the CBMC in [6].

## III. OTHER CONSIDERATIONS AND DESIGN PROCEDURE

### A. Class-AB Output Stage

When  $C_L$  is very large, e.g., in the order of nanofarads, the SR of an amplifier should be limited at the output stage. Hence, it is highly desirable to configure the output stage of a wide-range  $C_L$  amplifier in a class-AB mode. The employed class-AB output stage [9] relies on  $C_{bat}$  working as a level shifter (i.e., a floating battery) to propagate voltage variations at the gate of  $M_9$  to that of  $M_{10}$ . The accuracy of the voltage transfer demands both large  $C_{bat}$  and small parasitic capacitance at the gate of  $M_{10}$ . Unlike the realizations in [8] and [9] that connect the gate of  $M_{10}$  to that of  $M_3$ ,  $M_{10}$  is separately biased by  $M_{b3}$ , which can be sized with a smaller channel length than that of  $M_3$ , considerably reducing the parasitic capacitance. The transconductance of  $M_{10}$  can be thus more efficiently utilized. In addition, a large  $C_{bat}$  is beneficial to boost the gain at low frequencies. In the layout design, the top plate of  $C_{bat}$  is connected to the gate of  $M_{10}$ , reducing the added parasitic capacitance.

The saturation voltage of  $M_9$  should be sized the same as that of  $M_{10}$ , so that they can provide the same amount of

(dis)charging current during transients to obtain a symmetrical SR. In addition, a relatively low saturation voltage, which is another reason to bias  $M_{10}$  independently, benefits the voltage spike reduction at the input of the output stage, decreasing or avoiding the conduction of parasitic diode in  $M_R$  and itself.

### B. Noise

For simplicity, only thermal noise is accounted since the same method can be applied to analyze the flicker noise. As the noise contribution from the output stage, such as  $M_9$ ,  $M_{10}$ , and  $M_R$ , is greatly suppressed by the gain of the first stage, the input-referred noise is dominated by the first stage and can be given by

$$\overline{v_{n,T}^2} = \frac{8\kappa_B T \gamma}{g_{m1}} \left[ 1 + \frac{g_{m3}}{g_{m1}} + \frac{g_{m7}}{g_{m1}} \left( 1 + \frac{g_{m7} R_b}{2\gamma} \right) \right]. \quad (12)$$

Since  $R_b$  forms a shunt feedback between the gate and the drain of  $M_7$ , its noise voltage is directly amplified by  $M_8$  and adds at the first stage's output, which manifests as the last term in (12). Thus,  $R_b$  cannot be chosen too large to significantly degrade the noise performance. In this design,  $R_b$  adds 36.5% input-referred thermal noise.

### C. Design Procedure

There are several performance tradeoffs when  $C_L$  is varying. It is desirable to have a clear design procedure to balance the metrics under a variety of  $C_L$ . The first step is to place the poles of the embeddable CM. To boost the  $PM_{LFL}$  and, hence, the low  $C_L$  drivability as much as possible,  $\omega_{p2}$  and  $\omega_{p3}$  are set to be equal, achieving a 45° PM for the LFL inside the embeddable CM itself. Then, resolving (2) results in

$$\omega_{p2} = \omega_{p3} = \frac{\tan PM_{LFL} + \sqrt{(\tan PM_{LFL})^2 + 4}}{2} \omega_{\mu}. \quad (13)$$

The next step is to determine the capacitor multiplication factor  $G_{mb}R_b - 1$ . At nominal  $C_L$ , e.g., 100 pF in this design, the amplifier follows the overall transfer function in (6).  $PM_{overall}$  is recalculated with  $\omega_{p2} = \omega_{p3}$  and given by

$$PM_{overall} \approx 90^\circ - \tan^{-1} \frac{GBW}{\omega_{\mu}} + \tan^{-1} \frac{G_{mb}R_b + 1}{2} \frac{GBW}{\omega_{p2}} - \tan^{-1} \frac{GBW}{1 - \left(\frac{GBW}{\omega_{p2}}\right)^2}. \quad (14)$$

With specified  $PM_{LFL}$ ,  $PM_{overall}$ , and  $GBW/\omega_{\mu}$ ,  $G_{mb}R_b$  can be evaluated by simultaneously solving (13) and (14). For example,  $PM_{LFL}$  and  $PM_{overall}$  target 80° and 65°, respectively, while  $\omega_{\mu, Proposed}$  is set to roughly  $1.5 \times GBW$ ,  $G_{mb}R_b$  is  $\sim 4$  in this design. The minimum  $C_b$  is determined from the estimated  $C_{pb}$ ,  $C_{p1}$ , and  $g_{o1}$  to maintain  $PM_{overall\_min} > 45^\circ$ . Consequently, the estimated values of  $G_{m1}$ ,  $G_{mb}$ , and  $G_{mL}$  are calculated according to the expressions of  $GBW$ ,  $\omega_{\mu}$ , and  $\omega_{p2}$ . Following the aforementioned steps, the key parameters of the proposed amplifier are  $G_{m1} = 33.4 \mu S$ ,  $G_{mb} = 103.8 \mu S$ , and  $G_{mL} = 428.9 \mu S$ , respectively. The typical value of  $C_b$  is set to be 0.556 pF, with  $R_b$  being 38.5 kΩ, targeting a  $GBW$  of  $\sim 3$  MHz at  $C_L = 100$  pF.

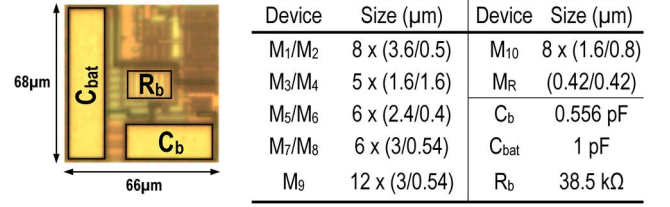


Fig. 4. Die photo of the amplifier (left) and its key device sizes (right).

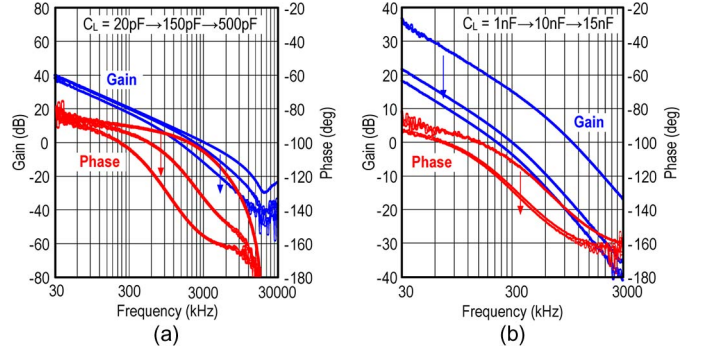


Fig. 5. Measured ac responses of the proposed two-stage amplifier at (a)  $C_L = 20, 150,$  and  $500$  pF. (b)  $C_L = 1, 10,$  and  $15$  nF.

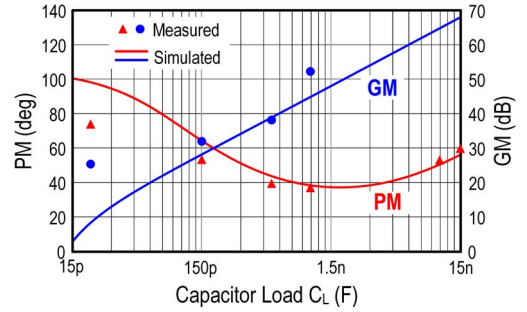


Fig. 6. Measured and simulated PM and GM curves over a wide range of  $C_L$ . The discrepancy at small  $C_L$  is likely due to the uncertain capacitances of the PCB traces and testing cables.

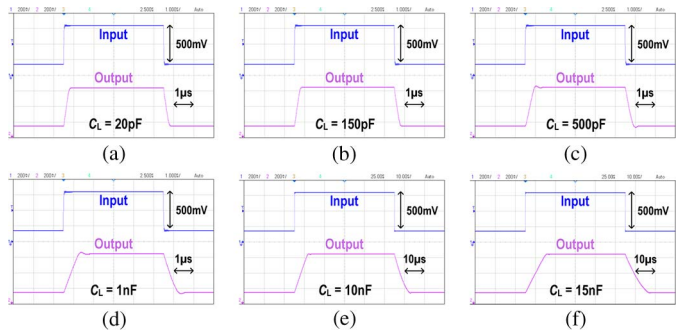


Fig. 7. Measured 500-mV step responses at: (a)  $C_L = 20$  pF; (b)  $C_L = 150$  pF; (c)  $C_L = 500$  pF; (d)  $C_L = 1$  nF; (e)  $C_L = 10$  nF; and (f)  $C_L = 15$  nF.

## IV. MEASUREMENT RESULTS

The amplifier was fabricated in 0.18-μm CMOS (see Fig. 4), and the die size is 0.0045 mm<sup>2</sup>, which is dominated by  $C_{bat}$  rather than  $R_b$  and  $C_b$  in the embedded CM compensation.  $C_{bat}$  and  $C_b$  are metal-insulator-metal capacitors.  $R_b$  is made

TABLE I  
PERFORMANCE SUMMARY AND COMPARISON

	This Work						JSSC'13 [4]				ISSCC'14 [10]
Technology	0.18 $\mu\text{m}$ CMOS						0.35 $\mu\text{m}$ CMOS				0.18 $\mu\text{m}$ CMOS
Chip Area ( $\text{mm}^2$ )	0.0045						0.016				0.007
Power @ $V_{DD}$ ( $\mu\text{W}$ )	32.4 @ 1.2 V						144 @ 2 V				6.3 @ 0.9 V
Estimated DC Gain (dB)	82						>100				>100
Input-Referred Noise Density ( $\text{nV}/\sqrt{\text{Hz}}$ @ 100 kHz)	130						174				N/A
Capacitive Load $C_L$ (pF)	20	150	500	1,000	10,000	15,000	1000	5,000	10,000	15,000	500
UGF (MHz)	3.06	2.26	1.41	1.05	0.30	0.22	1.37	1.24	1.06	0.95	1.34
Phase Margin ( $^\circ$ )	74.0	53.4	39.5	37.0	53.1	59.8	83.2	69.8	57.2	52.3	52.7
Gain Margin (dB)	25.4	32	38.2	52.3	>60	>60	9.8	16.6	17.0	18.1	N/A
Average SR ( $\text{V}/\mu\text{s}$ )	1.76	1.77	1.26	0.75	0.076	0.049	0.59	0.50	0.30	0.22	0.62
Average 1% $T_S$ ( $\mu\text{s}$ )	0.36	0.35	0.70	1.20	6.98	11.0	1.28	1.71	3.66	4.49	1.12
FOM <sub>S</sub> (MHz pF/mW) *	1,889	10,463	21,759	32,407	92,593	101,852	9,514	43,056	73,889	98,656	106,349
FOM <sub>L</sub> ( $\text{V}/\mu\text{s}$ pF/mW) #	1,086	8,194	19,444	23,148	23,457	22,685	4,097	17,326	20,833	22,917	49,206

\*FOM<sub>S</sub> = (GBW · C<sub>L</sub>) / Power #FOM<sub>L</sub> = (SR · C<sub>L</sub>) / Power

up of high-resistive polyresistors. The static current excluding the bias circuitry is 27  $\mu\text{A}$  at 1.2 V. The wide- $C_L$  drivability is verified in the frequency domain first, as shown in Fig. 5(a) and (b). With  $C_L = \sim 20$  pF [input capacitance of the equipment, electrostatic discharge, and printed circuit board (PCB) trace], the GBW reaches 3.06 MHz and the PM is 74 $^\circ$ , but the gain margin (GM) is 25.4 dB due to the reduced  $PM_{LFL}$ . When  $C_L$  is increased to 500 pF, the GBW is reduced to 1.41 MHz. The measured PM (39.5 $^\circ$ ) is close to the simulated value, which is  $\sim 44^\circ$ . At 1-nF  $C_L$ , the amplifier approaches to the minimum PM condition with the measured 37.0 $^\circ$  PM having  $< 2^\circ$  deviation from the simulation result. The measured GM is 38.2 dB. When  $C_L$  is further increased to 15 nF, the PM starts to recover with a value of 59.8 $^\circ$ , while the GM is  $> 60$  dB. The overall tendency is plotted in Fig. 6, which aligns well with the simulations.

The transient settling behaviors of the amplifier are verified via a 500-mV step stimulus. For  $C_L = \sim 20$  pF [see Fig. 7(a)], there exhibit no overshoot and ringing, indicating that the amplifier is adequately stable and consistent with the results given in Fig. 5. The measured positive and negative SRs are respectively 1.84 and 1.67  $\text{V}/\mu\text{s}$ , which are dominated by the current to (dis)charge  $C_b$ . When  $C_L$  is increased to 1 nF [see Fig. 7(d)], the output response shows both overshoot and undershoot, but their magnitudes are only  $\sim 3\%$ . The SRs are determined by the maximum amount of dynamic current provided by the output stage, which correspond to 0.712  $\text{V}/\mu\text{s}$  for the positive and 0.789  $\text{V}/\mu\text{s}$  for the negative steps. As  $C_L$  is as large as 10 nF [see Fig. 7(e)] and 15 nF [see Fig. 7(f)], the outputs become more and more stable. Particularly at  $C_L = 15$  nF, there is no visible ringing, overshoot, or undershoot. The SRs are proportionally reduced by  $\sim 15\times$ . The detailed performances are summarized in Table I and compared with recent advanced three-stage works. At large  $C_L$ , the UGF and PM of the proposed amplifier show relatively large variation in comparison with that in [4]. However, they may not be crucial for sensor interface applications. Rather, the proposed amplifier achieves the widest  $C_L$  drivability and occupies the smallest die area, while the FOM<sub>S</sub> and FOM<sub>L</sub> stay competitive at various  $C_L$  values.

## V. CONCLUSION

In order to enlarge the  $C_L$  drivability of a two-stage amplifier with small power and area, an improved version of embedded CM frequency compensation has been introduced. The first stage of the amplifier features the embedded CM minimizing the size of the physical compensation capacitors, improving the SR, and creating a useful LHP zero to enhance the stability. No extra bias circuit and power are required by the embedded CM. Detailed analytical treatments, design procedure, and silicon verification validated the feasibility of the proposed amplifier.

## REFERENCES

- [1] R. F. B. Turner, D. J. Harrison, and H. P. Baltes, "A CMOS potentiostat for amperometric chemical sensors," *IEEE J. Solid-State Circuits*, vol. SSC-22, no. 6, pp. 473–478, Jun. 1987.
- [2] W.-J. Huang, S. Nagayasu, and S.-I. Liu, "A rail-to-rail class-B buffer with DC level-shifting current mirror and distributed Miller compensation for LCD column drivers," *IEEE Trans. Circuits Syst. I, Reg. Papers*, vol. 58, no. 8, pp. 1761–1772, Aug. 2011.
- [3] R. G. H. Eschauzier and J. H. Huijsing, *Frequency Compensation Techniques for Low-Power Operational Amplifiers*. Dordrecht, The Netherlands: Kluwer, 1995.
- [4] Z. Yan, P.-I. Mak, M.-K. Law, and R. P. Martins, "A 0.016-mm<sup>2</sup> 144- $\mu\text{W}$  three-stage amplifier capable of driving 1-to-15 nF capacitive load with  $> 0.95$  – MHz GBW," *IEEE J. Solid-State Circuits*, vol. 48, no. 2, pp. 527–540, Feb. 2013.
- [5] P. R. Gray, P. J. Hurst, S. H. Lewis, and R. G. Meyer, *Analysis and Design of Analog Integrated Circuits*, 5th ed. Hoboken, NJ, USA: Wiley, 2009, pp. 643–649.
- [6] R. J. Reay and G. T. A. Kovacs, "An unconditionally stable two-stage amplifier," *IEEE J. Solid-State Circuits*, vol. 30, no. 5, pp. 591–594, May 1995.
- [7] G. A. Rincon-Mora, "Active capacitor multiplier in Miller-compensated circuits," *IEEE J. Solid-State Circuits*, vol. 35, no. 1, pp. 26–32, Jan. 2000.
- [8] Z. Yan, P.-I. Mak, and P. R. Martins, "Two-stage operational amplifiers: Power-and-area efficient frequency compensation for driving a wide range of capacitive load," *IEEE Circuits Syst. Mag.*, vol. 11, no. 1, pp. 26–42, Jan.–Mar. 2011.
- [9] J. Ramirez-Angulo, R. G. Carvajal, J. A. Galan, and A. J. Lopez-Martin, "A free but efficient low-voltage class-AB two-stage operational amplifier," *IEEE Trans. Circuits Syst. II, Exp. Briefs*, vol. 53, no. 7, pp. 568–571, Jul. 2006.
- [10] W. Qu, J.-P. Im, H.-S. Kim, and G.-H. Cho, "A 0.9 V 6.3  $\mu\text{W}$  multistage amplifier driving 500 pF capacitive load with 1.34 MHz GBW," in *Proc. IEEE ISSCC Dig. Tech. Papers*, Feb. 2014, pp. 290–291.